Nuclear Materials and Energy 18 (2019) 131–140

Contents lists available at ScienceDirect

Nuclear Materials and Energy

journal homepage: www.elsevier.com/locate/nme

Impact of ICRF on the scrape-off layer and on plasma wall interactions: From present experiments to fusion reactor

V. Bobkov[a,*], D. Aguiam[b], R. Bilato[a], S. Brezinsek[c], L. Colas[d], A. Czarnecka[e], P. Dumortier[f], R. Dux[a], H. Faugel[a], H. Fünfgelder[a], Ph. Jacquet[g], A. Kallenbach[a], A. Krivska[f], C.C. Klepper[h], E. Lerche[f], Y. Lin[i], D. Milanesio[k], R. Maggiora[k], I. Monakhov[g], R. Neu[a,l], J.-M. Noterdaeme[a,m], R. Ochoukov[a], Th. Pütterich[a], M. Reinke[h], W. Tierens[a], A. Tuccillo[n], O. Tudisco[n], D. Van Eester[e], J. Wright[i], S. Wukitch[i], W. Zhang[a], the ASDEX Upgrade Team[1], the Alcator C-Mod Team, the EUROfusion MST1 Team[2], JET contributors[3]

[a] Max-Planck-Institut für Plasmaphysik, Boltzmannstr. 2, 85748 Garching, Germany
[b] Instituto de Plasmas e Fusão Nuclear, Instituto Superior Técnico, Universidade de Lisboa, 1049-001 Lisboa, Portugal
[c] Forschungszentrum Jülich GmbH, Institut für Energie- und Klimaforschung, Plasmaphysik, Partner of the Trilateral Euregio Cluster (TEC), 52425 Jülich, Germany
[d] CEA, IRFM, F-13108 Saint-Paul-Lez-Durance, France
[e] Institute of Plasma Physics and Laser Microfusion, Hery 23 Str., 01-497 Warsaw, Poland
[f] LPP-ERM-KMS, TEC Partner, Brussels, Belgium
[g] CCFE, Culham Science Centre, Abingdon, Oxon OX14 3DB, UK
[h] Oak Ridge National Laboratory, Oak Ridge, TN 37831-6169, USA
[i] Plasma Science and Fusion, Massachusetts Institute of Technology, Cambridge, MA, USA
[k] Politecnico di Torino, Italy
[l] Technische Universität München, Boltzmannstr. 15, 85748 Garching, Germany
[m] Applied Physics Department, University of Ghent, Ghent, Belgium
[n] ENEA, Frascati, Italy

ARTICLE INFO

Keywords:
ICRF
RF sheath
Power balance, Three-strap
3-strap
ASDEX upgrade
JET-ILW
A2 antenna
ILA
Sputtering
Field-aligned antenna
Alcator C-Mod

ABSTRACT

Recent achievements in studies of the effects of ICRF (Ion Cyclotron Range of Frequencies) power on the SOL (Scrape-Off Layer) and PWI (Plasma Wall Interactions) in ASDEX Upgrade (AUG), Alcator C-Mod, and JET-ILW are reviewed. Capabilities to diagnose and model the effect of DC biasing and associated impurity production at active antennas and on magnetic field connections to antennas are described. The experiments show that ICRF near-fields can lead not only to $E \times B$ convection, but also to modifications of the SOL density, which for Alcator C-Mod are limited to a narrow region near antenna. On the other hand, the SOL density distribution along with impurity sources can be tailored using local gas injection in AUG and JET-ILW with a positive effect on reduction of impurity sources. The technique of RF image current cancellation at antenna limiters was successfully applied in AUG using the 3-strap AUG antenna and extended to the 4-strap Alcator C-Mod field-aligned antenna. Multiple observations confirmed the reduction of the impact of ICRF on the SOL and on total impurity production when the ratio of the power of the central straps to the total antenna power is in the range $0.6 < P_{cen}/P_{total} < 0.8$. Near-field calculations indicate that this fairly robust technique can be applied to the ITER ICRF antenna, enabling the mode of operation with reduced PWI. On the contrary, for the A2 antenna in JET-ILW the technique is hindered by RF sheaths excited at the antenna septum. Thus, in order to reduce the effect of ICRF power on PWI in a future fusion reactor, the antenna design has to be optimized along with design of plasma-facing components.

* Corresponding author.
E-mail address: bobkov@ipp.mpg.de (V. Bobkov).
[1] See the appendix of "A. Kallenbach et al., 2017 Nucl. Fusion 57 102015".
[2] See the author list of "H. Meyer et al., 2017 Nucl. Fusion 57 102014".
[3] See the author list of "X. Litaudon et al., 2017 Nucl. Fusion 57 102001".

https://doi.org/10.1016/j.nme.2018.11.017
Received 26 July 2018; Accepted 22 November 2018
Available online 20 December 2018

1. Introduction

Over the course of the last decade, many of the fusion experiments with magnetic confinement have been using Plasma Facing Components (PFCs) made of metallic materials, thereby partially or fully covering the first wall with more reactor-relevant high-Z elements. This has caused special attention to the studies of the impact of ICRF (Ion Cyclotron Range of Frequencies) power on the SOL (Scape-Off Layer) plasma and on plasma-wall interactions (PWI). Whereas the strongest consequence of these interactions for low-Z PFCs has been the increased heat loads at the elements close to ICRF antennas [1,2], the increased impurity content in the confined plasma has been exposed as a major concern for the application of ICRF power in a high-Z environment. This substantiated the studies at Alcator C-Mod [3,4], at ASDEX Upgrade (AUG) [5,6] and in JET with ITER-Like Wall ("-ILW") [7,8] which resulted in significantly better understanding of the ICRF adverse effects and development of successful methods to avoid them. This paper summarizes recent findings in these machines related to the ICRF-specific impurity production. Firstly, the progress of diagnostics and ways to model the impact of ICRF on the SOL and PWI are revisited. Secondly, the paper highlights how to apply the experience and the developed techniques to mitigate that in JET-ILW, ITER and perhaps in the perspective, DEMO.

2. Impact of ICRF on SOL and PWI: phenomenology, diagnostics and ways to model

2.1. Plasma biasing

In this paper, we consider the influence of electrostatic biasing of the SOL plasma to elevated positive voltages driven by ICRF fields at DC-grounded elements [9]. This phenomenon was found sufficient so far to explain the majority of the detrimental effects related to ICRF power, although additional players such as ponderomotive force [10], fast-particle induced PWI etc. cannot be fully excluded. We assume the standard "Radio-Frequency (RF) sheath rectification" hypothesis. The RF sheath paradigm in its simplified form implies the application of an electrical RF field with a component parallel to the equilibrium magnetic field $E_{||,\mathrm{RF}}$ and is closely related to the electrode or the plasma biasing in capacitively coupled RF reactors used for plasma processing [11]. Highly mobile electrons driven by $E_{||,\mathrm{RF}}$ are lost at the PFC surfaces until the RF sheaths are formed which compensate the electron losses and maintain plasma quasi-neutrality far from the surfaces, providing the drop of electrical potential which accelerates ions towards the surfaces. This plasma biasing is generally not a local phenomenon. Two main general routes exist for its propagation within the dimensions of the ICRF antenna and away from the antenna: (a) spreading of the RF-enhanced DC potential drop V_{DC} along the magnetic field lines; (b) wave propagation, with single or multiple wave modes involved, and consequent sheath rectification at other locations. Thus the plasma biasing can take place not only in the vicinity of the antennas, but also further away. The field component $E_{||,\mathrm{RF}}$ is associated with the so-called "Slow Wave" (SW) mode, which is evanescent at high plasma density ($> \sim 10^{17}$ m^{-3}), and propagates along the magnetic field lines. The so-called "Fast Wave" (FW) mode, evanescent at low density (<FW cut-off density of $\sim 10^{18}$ m^{-3}), is the mode used in common ICRF scenarios, in order to transfer the ICRF power perpendicularly to the magnetic field to the plasma core.

Fig. 1 presents a graphical scheme for the qualitative description of the propagation of the SOL perturbation induced by ICRF fields, with the AUG 2-strap antenna [12] geometry acting as an example. RF fields excited by the antenna emit the SW and the FW modes which propagate or decay evanescently within the antenna and within the torus. Thus the RF "near-fields", i.e., the fields in the vicinity of the antenna, are a superposition of the RF fields directly emitted by the antenna and those of the propagating or decaying waves coinciding with the antenna PFC surfaces. The incident waves get reemitted at the PFCs with a new field distribution between the wave modes depending on the local non-linear boundary conditions, e.g. a fast wave can be converted to a slow wave with high $E_{||,\mathrm{RF}}$. The RF "far-fields", i.e., RF fields far from antenna, are excited at the remote PFCs by the wave modes, which are not fully absorbed in the core or at the edge and are circulating inside the vessel [13]. The RF far-fields make in-vessel components effectively a re-emitting RF antenna, albeit typically with lower field amplitudes compared to the near-fields in the close antenna proximity. The near-fields can to some extent be characterized with the help of the RF current measurements at the antenna [14], whereas the RF magnetic field components of the far-fields can be measured by the B-dot probes distributed inside the vessel [15]. In addition to the RF fields, the RF-enhanced potential drop V_{DC} distributes itself along the field lines due to high parallel conductivity, either on the connections to active antennas or on those to the reemitting in-vessel structures. The concept of the emitted and reemitted waves is used here for simplicity. In fact, due to the non-linear nature of RF sheaths, the wave field distribution close to PFCs cannot be generally separated into purely incident and emitting components.

The potential drop V_{DC} can be estimated by several techniques. Use of the emissive probes [16], as in Alcator C-Mod [13] usually measuring the potentials of several hundred volts for MW-range of ICRF power, is one of the best-suited methods. This is because the probe acquires the plasma potential even if it is oscillating on the RF time scale, and the probe perturbation to the plasma is minimal. However this method is rarely accessible due to technical difficulties, such as those due to the $j \times B$ forces acting on the probe filaments. Under the conditions of small RF oscillations at the probe position, which imply strong SW evanescence and a good FW absorption, other probe techniques, such as Retarding Field Analyzer (RFA) can be used. The RFA probe data allows to obtain the averaged parallel ion energy $\langle W_{||,i} \rangle$ along the magnetic field lines connected to an active ICRF antenna, a measure of V_{DC} [17]. A combination of q_{95} scans and probe radial reciprocations [18] provides the possibility to characterize a 2D radial-poloidal area of the antenna. This can be seen in Fig. 2, where $\langle W_{||,i} \rangle$ for the AUG 2-strap antenna [19] powered by 600 kW is shown, measured on the field lines reaching from the probe position to the *R-Z* plane illustrated in Fig. 1. The corresponding $\langle W_{||,i} \rangle$ of up to 180 eV are significantly higher and inhomogeneously distributed, compared to that fairly constant of ~30 eV for the purely ohmic heating case. The biasing effect imposes changes of all components of the DC electric field E_{DC} in the SOL due to spatial variation of the DC biasing. Analysis of the Gas-Puff Imaging (GPI) diagnostics was adopted in Alcator C-Mod [20,21], to measure the velocity of density fluctuations advected by SOL flows. This provides information on the SOL DC radial electric field $E_{\mathrm{r,DC}}$ which can be integrated along radial paths to estimate the DC plasma potential V_{DC} (see also Section 3.1). Other promising techniques are under development, such as the purely non-perturbative spectroscopic diagnostics to measure electric fields inside the sheaths via modifications of the spectral line profiles due to the Stark effect [22,23].

Electromagnetic (EM) modeling has been improved recently, enabling calculations of RF near-field distributions with high spatial resolution, using finite-elements codes such as ANSYS HFSS [5], TOPICA [24] or COMSOL based codes for AUG [25,26], JET [27,28] and Alcator C-Mod antennas [29]. These, however, usually do not fully resolve the SOL wave propagation schematically described above. A more resource-demanding time-difference approach, with future prospects of implementing the non-linear RF sheath characteristics, was applied to model the Alcator C-Mod and ITER antennas [30]. For the RF sheath modeling, the SSWICH code has been applied which includes its versions with models describing the slow-wave ("-SW") [31] and the more realistic full-wave [32] propagation in the SOL self-consistently with the non-linear "RF sheath boundary condition" [33]. The SSWICH code provided theoretical profiles of V_{DC} in front of the AUG [6] and the JET [27,28] antennas. These were found qualitatively consistent with the

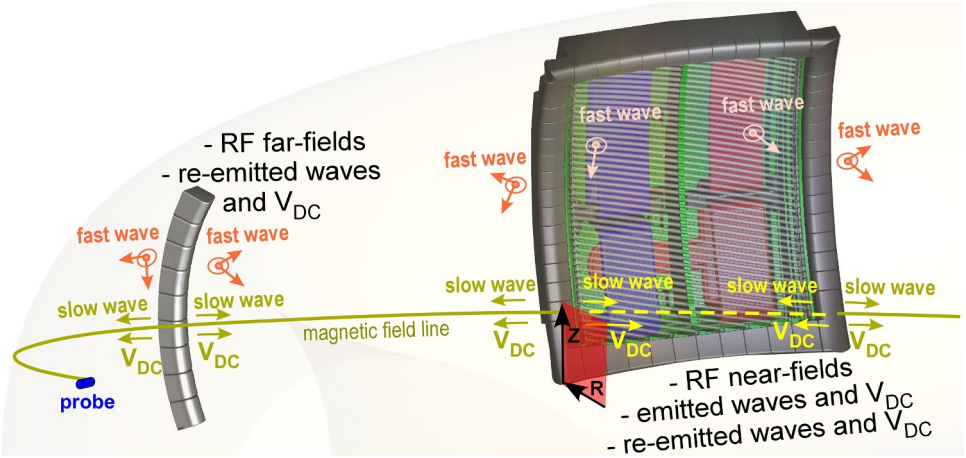

Fig. 1. Schematic presentation of the propagation of the SOL plasma biasing close to and away from an ICRF antenna. A magnetic field line is illustrated connecting the antenna to other structures and diagnostics in the vessel.

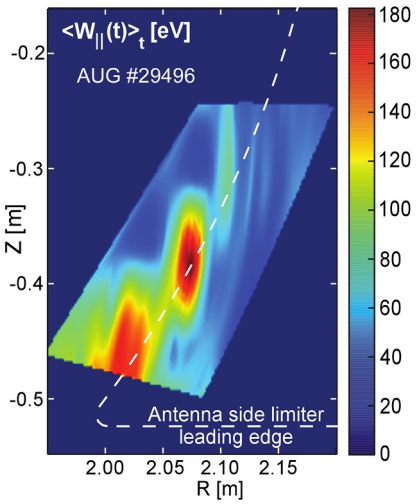

Fig. 2. $\langle W_{||,i} \rangle$ due to plasma biasing on the field lines connected to the 2-strap AUG antenna, adopted from [19].

experimental data. Two main approximations need to be relaxed for further modeling improvements. Firstly, the wave propagation including resonances close to antennas need to be resolved along with excitation of additional wave modes. Currently, in particular the lower hybrid resonance is often avoided in calculations by using vacuum or plasma layers with a minimum density, making the near-field modeling less realistic. The above mentioned time-domain approach and newly developed codes or those under development, e.g., ERMES [34], could be used to overcome these limitations. Secondly, the full wave absorption boundary conditions used currently in the above-mentioned codes is a too strong approximation for the cases when modeling of the full in-vessel RF-field distribution is required, e.g. for the far-field estimation. Coupling of the core wave codes with the codes describing the SOL plasma and antenna, as described in [35], will allow more realistic far-field and near-field calculations, with the RF power circulation in full toroidal 3D toroidal geometry incorporated.

2.2. $E \times B$ convection in the SOL: density and transport modifications

The E_{DC} field can impose $E \times B$ drifts in the far SOL, in addition to the convection associated with turbulent blob-like inhomogeneous plasma formations on the open magnetic field lines [36,37]. However, observations of the E_{DC}-induced effects are often not universal for different experiments, likely due to large differences in the SOL properties, such as neutral penetration and radial ionization profile. In Alcator C-Mod, although the $E \times B$ convection is present and is well-characterized [21], density modifications are limited to the region within several mm in front of the antenna face [38]. This is in contrast to the AUG and the JET-ILW observations, where significant modifications of the SOL plasma density are evidenced on the scale of radial extension of several centimeters, as will be described below. Further, recent studies of the modifications of the SOL transport properties in Alcator C-Mod and in JET will be summarized.

Experimental observations of the density modifications obtained in AUG and JET-ILW are shown in Fig. 3. In Fig. 3(a, top), the modifications of the ion saturation current I_{sat} related to the density perturbation induced by ICRF fields [19] is shown for the probe measurements on the field lines connected to the AUG 2-strap antenna, in the same geometry as in Fig. 2. The region in the lower part of the antenna, characterized by high $\langle W_{||,i} \rangle$ and V_{DC}, experiences at the same time density depletion. A similar depletion effect takes place also on the upper part of the AUG 3-strap antennas [39] with non-optimized power balance of the RF feeding (see also Section 3), as n_e-profiles obtained with the help of the antenna embedded reflectometry [40] demonstrate in Fig. 3(a, bottom) [41]. In JET-ILW, Li-beam diagnostics shown in Fig. 3(b, left) provides similar information for the field lines connected to the so-called A2 antenna [42] or to the ITER-Like Antenna (ILA) [43]. In Fig. 3(b, right), the inhomogeneous perturbation of the density distribution, mapped along magnetic field lines to the ILA, corresponds to the time window when this antenna is turned on. For JET, in the absence of the diagnostics measuring V_{DC}, the observations of the density modifications provide valuable indirect information on the associated plasma biasing effect and on the PFC areas connected along the field lines to the region perturbed by ICRF, where PWI can take place (see Fig. 3(b, left) for the areas on the Low-Field Side (LFS) as well as on the High-Field Side (HFS)).

For AUG, the effect of the plasma biasing on the $E \times B$ driven convection and the density distribution was qualitatively reproduced in modeling [19]. The V_{DC} distribution based on the $\langle W_{||,i} \rangle$ measurements by the RFA probe (Fig. 2) was used as an input to the 3D edge plasma fluid code with kinetic transport model for neutrals EMC3-Eirene [44], which was modified by introducing the $E \times B$ drift terms in the fluid equations [19]. The I_{sat} distribution at the probe measurements location was then calculated, which agreed qualitatively well with the I_{sat} distribution measured (Fig. 3(a, upper)). A purely numerical iterative loop of simulations, involving RAPLICASOL and SSWICH-SW to calculate the V_{DC} distribution and then EMC3-Eirene with $E \times B$ drifts to calculate the modified density distribution, was established in [41]. The numerical loop of codes showed similar results to those obtained using the measured V_{DC} distribution: the strength of the density modifications

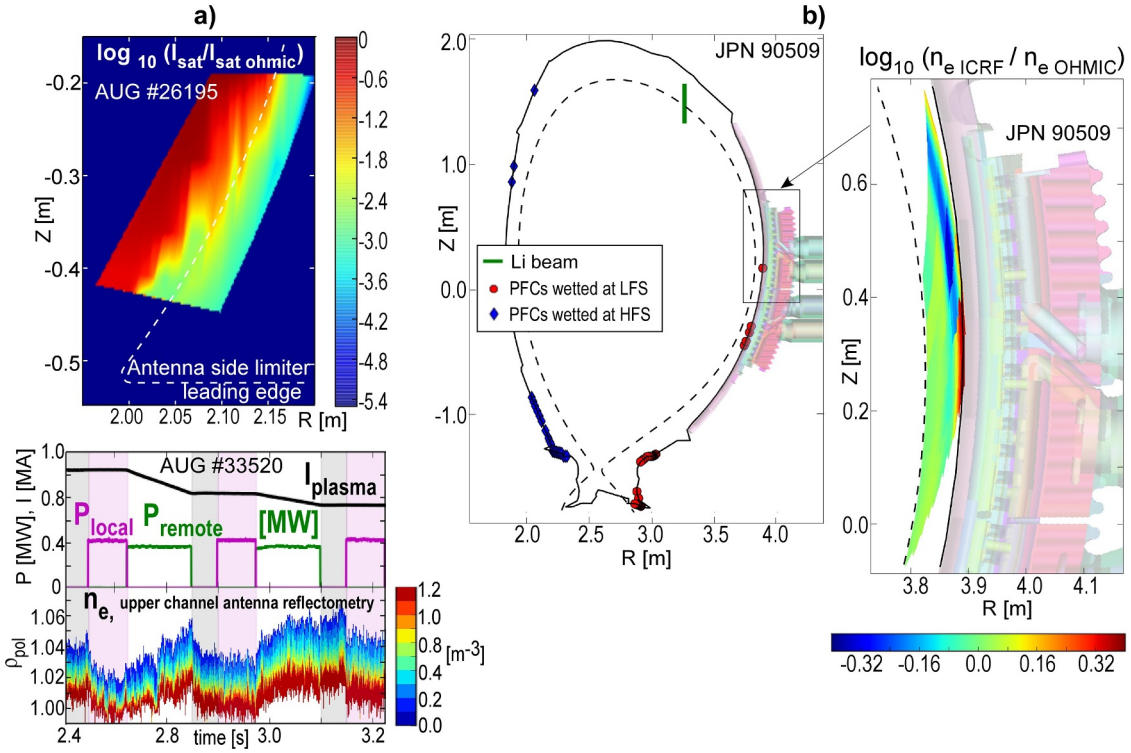

Fig. 3. Density modifications in the SOL in AUG (a) and in JET-ILW (b): (a) Top – ICRF-induced I_{sat} modifications w.r.t. ohmic case, setup as in Fig. 2, adopted from [19]; bottom – n_e-profile modifications measured by embedded antenna reflectometry during ohmic phases, local and remote ICRF power, adopted from [41]. (b) Left: JET-ILW cross-section with Li-beam diagnostics and field lines connections to wetted PFCs indicated; Right: n_e modifications measured by Li-beam and mapped to ILA [43].

depend on the amplitude of V_{DC} and its distribution is a function of the RF feeding of the 2-strap and the 3-strap antennas (see also Section 3).

The calculations of density modifications discussed above do not include effects of plasma turbulence. Turbulent plasma blob formations, moving radially towards the outer wall and the antennas, influence significantly the plasma parameters in the far SOL close to PFCs. The ICRF-induced E_{DC} can modify the structure and movement of blobs, as was shown using calculations in [45–47]. Furthermore, it has been suggested (see [48]) that the SOL transport properties, in particular the penetration probability of impurity ions across SOL radially towards plasma, can be modified by E_{DC}. This hypothesis has been examined experimentally, first in Alcator C-Mod [49,50] and later in JET-ILW [51]. Low-recycling N_2 gas was injected in locations close and far (with limited magnetic field connections) w.r.t. the active ICRF antennas. Spectroscopic measurements of multiply-ionized nitrogen levels in the confined plasma were used to estimate the effect of ICRF fields on the penetration probability while keeping the source of nitrogen constant. It was found in both experiments that the ICRF fields do not affect the relative levels of nitrogen in the plasma significantly. For JET-ILW, this result was confirmed for both the standard dipole RF feeding of the A2 antennas and for the -90° phasing feeding scheme. It was concluded that the transport modifications by the DC biasing effect, if present, do not influence penetration probability of impurities from the outer wall towards the confined plasma significantly, although the density distribution can still be affected by interactions of E_{DC} with turbulence. Thus, for the explanation of the increased impurity content associated with ICRF, the corresponding additional sources of impurities are of primary importance.

2.3. ICRF-related PFC sputtering

The increased ions energies can lead to physical sputtering of the PFC surfaces. In deuterium plasmas, at energies below the deuterium sputtering threshold of tungsten (*W*) of 230 eV, the ions of the intrinsic light impurities contribute most to the sputtering in AUG [5] and in JET-ILW [7]. For molybdenum (*Mo*) sputtering in Alcator C-Mod, the deuterium ions contribute dominantly if their energy is higher than the sputtering threshold of ~100 eV [52]. In the case of the heavier tritium, the sputtering threshold decreases accordingly, making the main ions the most likely dominant contributors, unless the ion energies are kept below ~150 eV for *W* and ~70 eV for *Mo* [53]. In the case of helium (*He*) plasma, the threshold energies are 120 eV for *W* and 60 eV for *Mo*. The acceleration voltage required to achieve these energies drops effectively by a factor of 2, if helium is doubly-ionized. The low sputtering thresholds make *He* one of the most challenging species to work with, while progressing towards minimization of the ICRF-related impurity production. This was indeed experienced in the *He*-experiments in AUG [6,54], where generally increased PWI was observed, affected in addition by the high fueling efficiency and low neutral pressure in the SOL.

A typical correlation of the increment of the *W*I spectral line intensity measured spectroscopically at the AUG antenna limiters and RF power in an H-mode discharge is shown in the upper part of Fig. 4. Production of W depends on the local density of intrinsic light impurity ions, such as oxygen, boron, carbon, nitrogen etc. (see [5] for description of the role of light impurities), and varies dramatically due to plasma turbulence, in particular during ELMs and ELM-like events. This results in large excursions in the observations of the spectral line intensity. The lower envelope of the intensity is reminiscent to that on the square root of power (i.e., on voltage). However, even assuming that the inverse photon efficiency required to translate the *W*I line intensity into the *W* influx [55], is approximately constant, the link between the RF power and the sputtering is highly non-linear. This link implies not only the rectification mechanism and the accompanying modifications of the local plasma parameters, but also the threshold-like sputtering behavior. The presence of multiple species of light impurities with a

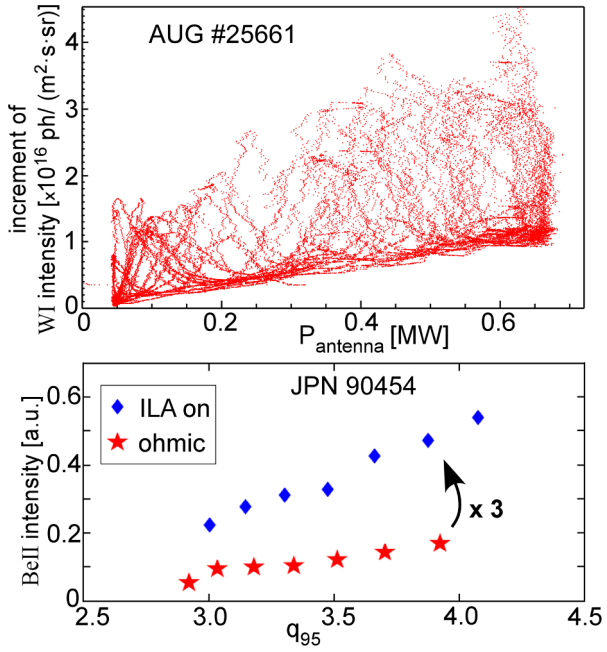

Fig. 4. Upper: Increment of *W*I line emission at the AUG 2-strap antenna limiter as a function of RF power. Lower: *Be*II line emission on outboard limiter magnetically connected to ILA (P_{ILA} = 1 MW), as function of q_{95} in JET-ILW, adopted from [56].

variation of charge states complicates the link even further.

In the lower part of Fig. 4, the *Be*II spectral line emission intensity on the outboard limiter connected magnetically to the ILA antenna in JET-ILW is shown for the ohmic and for the ILA-powered plasmas (P_{ILA} = 1 MW) as a function of q_{95} [56]. A drastic difference (about a factor of 3) compared to the ohmic case is observed when the ILA is active. Combined with the density modifications on the field line connections to active antennas described above, the observations of the Be sputtering hint to the fact that the ICRF-related *W* sources on the wetted *W* PFCs (indicated in Fig. 3(b)) are the likely causes for the elevated *W* content in ICRF heated plasmas in JET-ILW [7].

3. Tackling adverse effects of ICRF power

Ways to reduce the DC biasing effect, and notably the impurity production, have been elaborated in the recent years. Their implementation in existing devices was highly successful, showing good prospects for future devices.

3.1. Antenna design and RF feeding

Antenna design changes and tuning of the RF feeding to mitigate the near-field effects are proving best suitable ways to tackle the adverse effects of ICRF power. Various experimental observations in AUG, Alcator C-Mod and JET-ILW [1–7] are pointing out that the RF near-field effects make a stronger impact compared to the RF far-field effects. Two general approaches to modify antenna geometries, dedicated to the reduction of the impurity production by affecting the near-fields, have been recently tested experimentally in AUG and in Alcator C-Mod. Before describing these, the differences in setups of ICRF antenna PFCs at Alcator C-Mod and in AUG have to be highlighted. In Alcator C-Mod, the antenna guards – the private antenna limiters are retracted radially behind the main poloidal limiters located away from the antenna. In AUG, the antenna limiters are the main poloidal and toroidal limiters. Therefore the *Mo* sources away from the antenna are more important in Alcator C-Mod in typical plasmas, whereas for AUG the local *W* sources at the antenna are dominant, unless largely reduced.

A significant reduction of the ICRF-specific impurity production after replacing the old toroidally-aligned (TA) antennas by the so-called Field Aligned (FA) antenna [29] was observed in Alcator C-Mod [4]. However, no single effect accompanying the antenna geometry changes was confirmed to be responsible for the improvement including practically a complete elimination of impurity sources measured at the antenna. One of the contradicting observations was that the RF-enhanced plasma potential measured on the field lines connected to the lower corner of the FA antenna was not reduced compared to the potentials of the TA antenna. Nevertheless, the modifications of the near-field distribution, the $E \times B$ convection and properties of the magnetic connections to the antenna still remain among the main candidates to explain the impurity reduction. More importantly, the experiments with the FA antenna demonstrated that changes in antenna design can indeed be successfully applied to reduce the adverse effects of ICRF heating.

An independent route for antenna development was pursued in ASDEX Upgrade [5], involving management of the RF currents at the antenna PFCs. One of the common results from the near-field calculations (see e.g., [57,58]), is that $E_{||,RF}$ is affected by contributions from the antenna box excited by RF image currents. The approach relying on the reduction of the RF image current density and the associated near-fields was first tested experimentally by using the so-called “broad-limiter” 2-strap antenna [5]. In the experiments with this antenna [59], a lower *W* production was indeed observed, although the changed limiter geometry and extended shadowing of the antenna from the edge plasma could have an additional influence. A drastic reduction of the impurity generation was shown by using the novel 3-strap antenna design [38,59]. The configuration of the antenna straps makes it possible to reduce the RF currents on all the plasma facing side limiters at approximately the same parameters of the RF feeding close to the dipole strap phasing [6,59], when the RF image current contributions from the central strap are cancelled by those from the outer straps. Other elements, such as limiters and the Faraday Screen (FS), were built in the same way as for the old 2-strap antennas.

Fig. 5 shows that the local physical parameters at one of the antenna limiter tiles: (a) the toroidal component of the RF current $I_{rf\ tor}$ (representing the RF image current), (b) the rectified current I_{DC} (a measure of the intensity of the non-linear RF sheath - driven DC biasing) and (c) the increment of the *W* sputtering yield ΔY_W are strong functions of P_{cen}/P_{total} – the strap power balance parameter and of $\Delta\Phi$ – the deviation of the strap phasing from dipole (0/π/0). The power balance parameter is expressed as the ratio of the power launched by the central strap P_{cen} to the total power launched by the antenna P_{total}. Although such local characteristics show a variation of the optimal feeding parameters (minima of $I_{rf\ tor}$, I_{DC} and ΔY_W) from location to location (see [6,26] for details), the feeding optimization strongly reduces the integrated ICRF-specific *W* sources, as can be seen in Fig. 5(d). A distinctive minimum of the ICRF-specific increment of the *W* content in the plasma core Δc_W (at $T_e \approx 1.5$ keV) is observed when the central strap delivers about twice the power of both outer straps, i.e., $P_{cen}/P_{total} \approx 0.67$, and when the phasing is slightly shifted w.r.t the nominal dipole case $\Delta\Phi \approx 10^\circ$. In this H-mode discharge with constant P_{ICRF} = 1MW (2 antennas with P_{total} = 0.5 MW each) with hydrogen (*H*)-minority scheme at f_{AUG} = 30 MHz (see [26] for details), the *W* content at the minimum is reduced practically down to the background level with NBI heating only. The optimum power distribution between the straps can change depending on the scenario, frequency etc., and so far is found between P_{cen}/P_{total} = 0.55 and P_{cen}/P_{total} = 0.7. The level of Δc_W is significantly reduced compared to the *W*-coated 2-strap antennas and is approximately at the level of the boron-coated 2-strap antennas, except for the *He* operation where the 3-strap antennas show even lower *W* production in the comparison [6].

The method of the cancellation of the RF image currents at the antenna PFCs described above for the AUG 3-strap antenna, is applicable to some of the already existing antenna designs. This was

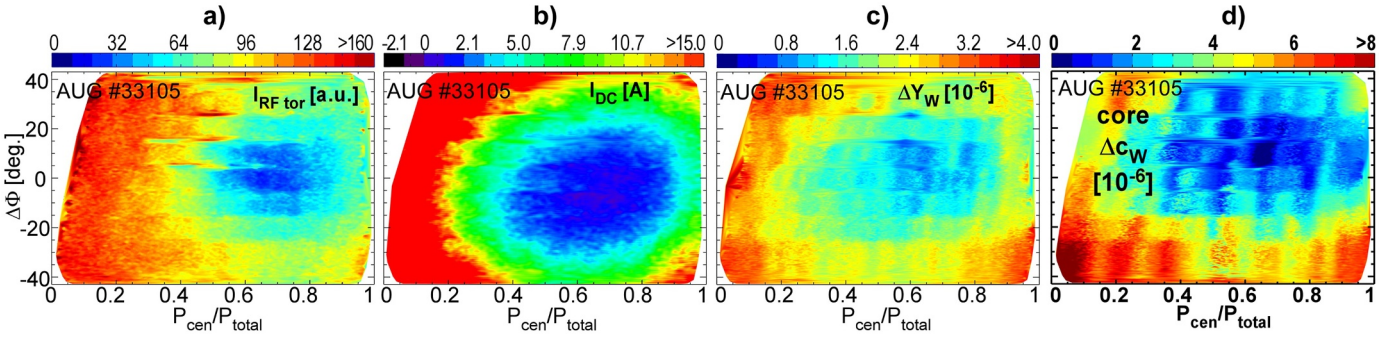

Fig. 5. RF feeding diagrams using strap power balance P_{cen}/P_{total} and phase deviation from dipole ΔΦ as variables in a discharge with P_{ICRF} = 1 MW; (a), (b), (c) – local measurements at a single antenna limiter tile (vertical position z ≈ 0.2, left limiter as seen from the plasma) of toroidal RF current $I_{rf\ tor}$ (a), DC current circulation I_{DC} (b) and increment of the *W* sputtering yield ΔY_W (c); d) increment of *W* content in plasma at T_e ≈ 1.5 keV.

confirmed in Alcator C-Mod during experiments with the 4-strap FA antenna [50]. For the FA antenna, the fixed dipole strap phasing 0/π/0/π phasing was used, i.e., when the RF current on every strap is out-of-phase to that on the neighboring strap(s). RF transmitter circuit provided the possibility to vary the power balance between the two central straps and the two outer straps. The *Mo*I line emission at the large area covering the antenna elements including the limiters and the Faraday screen (see [4] and references therein) showed a minimum of *Mo* source at the antenna for P_{cen}/P_{total} values between 0.5 and 0.8. No detectable difference of the local *Mo* sources between the standard FA operation at P_{cen}/P_{total} = 0.5 and other P_{cen}/P_{total} values in this range was measured. This range does indeed cover the situation when the RF image currents are mostly cancelled at the lateral sides of the antenna frame. However, as mentioned above, the local antenna *Mo* sources are less important in Alcator C-Mod compared to the sources remote to the antenna. The core *Mo* content, governed by the remote *Mo* sources, exhibited a strong dependence on the power balance P_{cen}/P_{total}. It was reduced around P_{cen}/P_{total} = 0.7, characteristic of RF image current cancellation at the lateral antenna elements. An even more appealing result was achieved using the GPI diagnostics measuring the poloidal component of the velocity of the turbulent formations on the field lines connected to the FA antenna. As mentioned in Section 2, the poloidal velocity is a measure of the radial component of the ICRF induced DC field in the far SOL $E_{r,DC}$ which is a V_{DC} proxy. At the values of P_{cen}/P_{total} of 0.7–0.9, the V_{DC} proxy on the field lines connected to the FA corner dropped to the level observed without ICRF power. This indicated that the RF-enhanced potential was locally completely eliminated.

The AUG and the Alcator C-Mod experiments prove that the reduction of the RF image currents at the antenna frame is a fairly robust method to reduce the RF-enhanced potentials and the impurity sources associated with the ICRF power, once the antenna design and operation provides the possibility to reduce the RF image currents simultaneously at most of the antenna PFCs. In Section 3.3 below, implications and possible future applications of this method will be discussed.

Independently from the experiments described above, differences in impurity production between the A2 antennas and the ILA [60] (which has fundamentally different design) were observed in JET-ILW. About 20% lower radiation and *W* production are consistently measured with the ILA compared to the A2 antenna at a fixed ICRF power in the same plasmas. The *W* sources in JET-ILW are located either in the divertor, or its entrance, or at the HFS. Thus the ILA produces smaller integrated *W* source at these locations, having a significantly smaller surface area and correspondingly higher (up to a factor of 4) power density. Several mechanisms are considered as candidates to explain this reduction, including the smaller wetted area of the magnetic connections and the less pronounced RF-enhanced DC biasing due to a more favorable EM design of the ILA PFCs. However, pinpointing the critical differences in the design is not straightforward. Efforts to compare the two antennas using the same boundary conditions in the calculations are underway and will be reported elsewhere.

3.2. Gas puffing for 3D tailoring of the SOL

Apart from the optimization of the antenna layout and of the RF feeding, the impurity production can be reduced by modifying the 3D properties of the SOL.

In particular, the 3D density distribution can be tailored by choosing the appropriate valve to inject the working gas. The rationale is to keep the core plasma parameters approximately constant, but affect the 3D distribution of neutrals in the far SOL to increase densities of neutrals and of plasma close to the antenna PFCs. This benefits both the coupling properties of the antenna [61] and lower sputtering at the PFCs, the latter being usually the case with [39] and as well as without [62] ICRF power. This technique can be easily used when the SOL is not very opaque to neutrals, which then can penetrate relatively far toroidally and poloidally before getting ionized, as is the case in AUG and in JET-ILW. Fig. 6 shows the values of the *W* influx Γ_W averaged over the limiters of an active *W*-coated 2-strap AUG antenna, for the cases with 5 different deuterium valves located in various toroidal sectors in AUG (overall 16 sectors), used with the same gas injection rate of 1.2×10^{22} el/s. The lowest local Γ_W is observed when the midplane gas valve closest to the Γ_W measurements is used, followed by the case when the injection location from the top of the vessel can produce higher density close to the Γ_W measurement region due to connections along magnetic field lines. The local *W* source is largest (with small variations) in the cases when the evenly distributed lower divertor gas injection, the top injection with limited magnetic connections and the midplane valve at the opposite side (w.r.t. measurements) of the torus are used. This

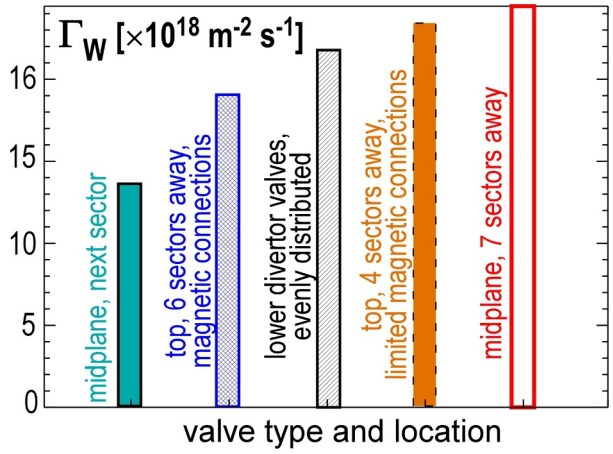

Fig. 6. Measurements of W sources averaged over the AUG antenna limiter, depending on the type of gas valve and its injection location.

picture agrees qualitatively with the 3D density distribution calculations by the EMC3-Eirene code. The calculations show that the local density at the antenna is highest if the midplane valve in the antenna vicinity injects gas [63]. The density can also be increased by the top valves, in particular by those which can form gas clouds on the low field side in the antenna vicinity or in the regions with a well-defined magnetic connection to the antenna [64]. Experiments in JET-ILW show fundamentally the same behavior of the RF coupling properties as in AUG, when divertor, top and midplane valves are used [61]. The JET-ILW experiments also highlight that the midplane valves are generally preferable to the divertor valves to reduce the *W* content when the core parameters are approximately constant [65], in agreement with similar AUG observations [66].

In Alcator C-Mod experiments, where the SOL is more opaque to neutrals, neither the effect of the local working gas injection on ICRF coupling, nor the effect on the ICRF-specific impurity production was observed, when changing the location of the working gas injection. At the same time, the experiments showed that a strong effect on the RF-enhanced potentials on the field lines connected to active antennas exists, when the whole SOL changes during light impurity injection [21]. Injection of He, N_2 and Ne effectively reduced the potentials estimated by the GPI techniques by about a factor of 2.

EMC3-Eirene calculations for local gas injection in ITER, where the SOL is also opaque to neutrals in the region close to the FW cut-off, were made recently [67]. The calculations indicate that with the planned geometry of the valves close to the ICRF antennas in ITER, the effect on the local density at the antennas is significant and could indeed improve ICRF coupling. Location and geometry of both the gas valves and the antennas PFCs are important: (a) the radial position and geometry of the surrounding components defines how neutrals penetrate in all directions before ionization, as the EMC3-Eirene calculations in [63,64,68] demonstrate; (b) the PFC configuration influences how the density profile forms in front of the antenna. The role of the later was observed in the experiments with the AUG 2-strap antenna with broad limiters. This antenna showed practically no response of the RF coupling properties to the local gas injection in H-mode plasmas [69], in contrast to the predecessor 2-strap antenna with standard limiters and the successor 3-strap antenna. This was likely due to the fact that the broad limiters shadowed the front of the antenna from the regions with dense neutrals and plasma. Similar to that, one of the fundamental differences in Alcator C-Mod compared to AUG and JET, is the positioning of the FW cut-off layer in the shadow of the antenna guards. This makes a change of the density profile close to the cut-off even more difficult. However, it still remains to be proven whether this technique is at all applicable to a case with the Alcator C-Mod SOL properties. EMC3-Eirene calculations can be applied in the future for the Alcator C-Mod cases to shed more light on the uncertainties.

3.3. Implications for other experiments, present and future

Recent experimental knowledge and advances in RF sheath theory elucidate guidelines to design an antenna with reduced impact on the SOL and PWI. Various experimental observations, in particular those on both sides of magnetic field lines connections (see [70] and references to the experiments therein), demonstrate, that the old rule of reduction of the electric field integrated along field lines $\int E_{||,RF}\, dl$ [71] is obsolete. Spatial proximity of the antenna PFCs (where RF sheath can form) to the $E_{||,RF}$ emitters is important [70]. Theoretical estimates in [32,70] also indicate that the wave propagation in the SOL often plays a limited role in affecting the RF near-fields. The SW is mostly evanescent under the usual ICRF coupling conditions and its effect on the near-field distribution is localized on spatial scales smaller than those of the antennas. The FW propagates mainly perpendicularly, forming a high power flux propagation cone directed radially towards the confined plasma [32]. Therefore toroidal and poloidal distances between the antenna PFCs and the high power flux regions should be maximized, in order to reduce the effect of the FW on $E_{||,RF}$ at PFC surfaces, where incident FWs can be mode converted to the SW with high $E_{||,RF}$.

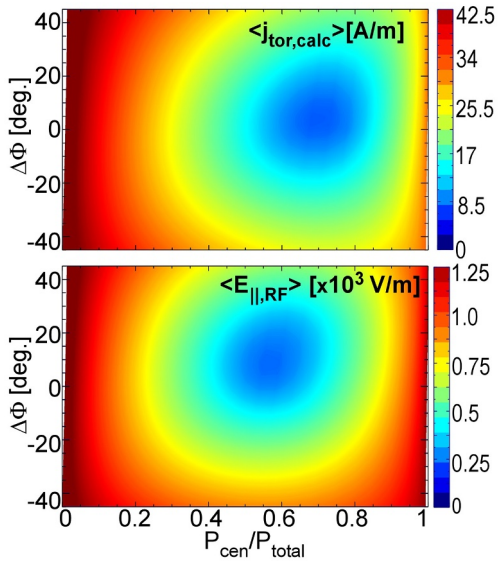

Fig. 7. TOPICA calculations of $j_{rf\ tor}$ and $E_{||,RF}$ at the location as in Fig. 5(a), $P_{total} = 0.5$ MW.

The general reduction of $E_{||,RF}$ close to the PFCs taking into account the wave fields constitutes the main guideline to reduce the impact of ICRF power on the SOL and PWI. Whereas the RF sheath simulations with the wave fields are required for quantitative estimates of $E_{||,RF}$ and V_{DC}, the EM modeling without the wave propagation (which requires less computing resources) can still be applied to develop and optimize antenna design and feeding schemes (see e.g., [72]). For this, $E_{||,RF}$ calculated near PFCs with the EM codes needs to be minimized, but keeping in mind the wave propagation features mentioned above.

Fig. 7 shows EM TOPICA calculations of the toroidal RF current density and the associated excitation of $E_{||,RF}$, averaged over the location of the AUG 3-strap antenna curved model [73] corresponding to the local measurements from Fig. 5(a), for the plasma conditions as in the experiment. The experimental picture of the minimum of the RF current is qualitatively well reproduced. Moreover, EM properties and the RF sheath characteristics modeled by SSWICH-SW in [6,26] agree with the experiments, giving confidence that the effect of the reduction of the RF image current can be used as recipe for antenna design and can be assessed theoretically for other antennas. Two antennas are currently of interest where this method can be applied in the future: the 4-strap A2 antenna operating in JET-ILW and the ICRF antenna in ITER designed to have 4 toroidal rows of straps.

For the JET A2 antenna, the L-mode plasma JPN 90454 with $f_{A2} = 42.5$ MHz and well-characterized edge plasma profiles is considered. Fig. 8(a) shows the A2 antenna TOPICA model. In Fig. 8(b), the values of $E_{||,RF}$ averaged over the PFC regions ($\langle E_{||,RF}\rangle$) for $P_{total} = 1$MW are shown: close to the poloidal limiters and to the A2 antenna specific septum.

At first, the same feeding scheme as that used for the Alcator C-Mod 4-strap antenna is examined: the standard dipole 0/π/0/π phasing. For this phasing and for the condition of maximum available power from the A2 antennas, the RF properties of the A2 antenna prescribe $P_{cen}/P_{total} \approx 0.3$ (working point "1") corresponding to equalized RF transmission line voltages. The minimum of $\langle E_{||,RF}\rangle$ at the limiters is found at $P_{cen}/P_{total} \approx 0.7$ and $\Delta\Phi = 10^\circ$ (working point "3"), corresponding to approximately 50% of maximum power available for working point "1". An intermediate case, corresponding to the equalized strap powers, with $P_{cen}/P_{total} \approx 0.5$ (working point "2"), with about 70% of the maximum available power, is of additional interest. The septum $\langle E_{||,RF}\rangle$ is approximately constant for these three working points (although the

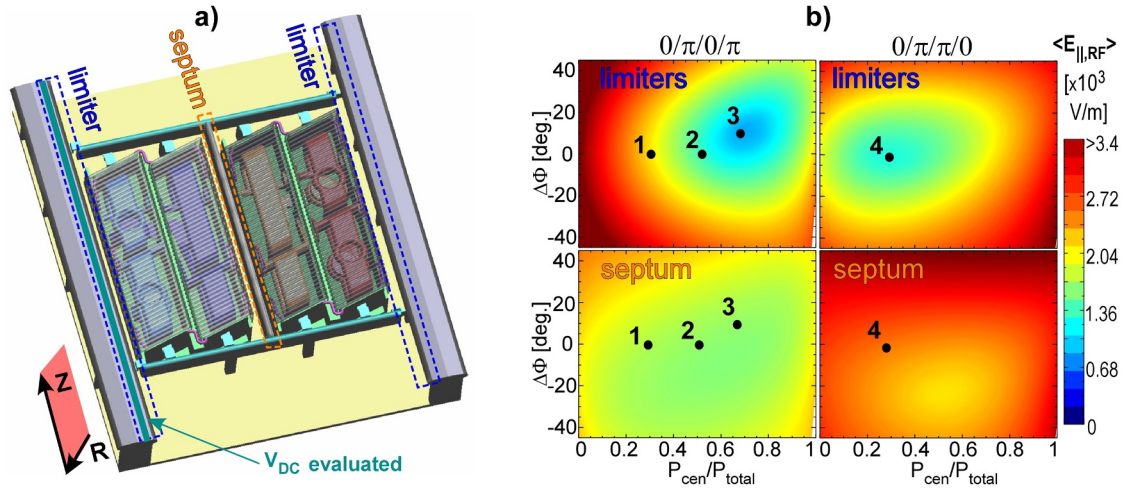

Fig. 8. (a) TOPICA model for the JET A2 antenna with regions close to PFCs highlighted; (b) RF feeding diagrams for $E_{||,RF}$ averaged over the regions from (a) for four working points (P_{total} = 1 MW).

spatial distribution changes), and it is the reason why achievable reduction of V_{DC} is limited (see below).

Another option shown in Fig. 8 has two inner straps operating in-phase, when using the 0/π/π/0 phasing. This RF feeding scheme has the advantage of minimized $\langle E_{||,RF}\rangle$ at the limiters at $P_{cen}/P_{total} \approx 0.3$ (working point "4"), when the maximum antenna power is available. However in this case, $\langle E_{||,RF}\rangle$ at the antenna septum is further increased compared to the working points with the 0/π/0/π phasing.

Fig. 9 shows the radial (R) – poloidal (Z) profiles of V_{DC} calculated by SSWICH-SW for the left lateral limiter of the antenna (calculations at other PFCs lead to the same conclusions as below). The figure presents V_{DC}-profiles for the four working points described above. The reduction of V_{DC} for the 0/π/0/π phasing working points "2" and "3" is accomplished only for the upper and the lower parts of the antenna and is accompanied by changes in V_{DC} distribution in the central part. For point "4", V_{DC} due to the contribution of the septum is even higher. Therefore the A2 antenna septum hampers the optimization of the RF image currents and makes it more difficult to reduce the impact of the RF near-fields on the SOL and PWI in JET-ILW. For the 0/π/0/π phasing at high P_{cen}/P_{total}, the increased out-of-phase RF image currents at the septum lead to distinctive peaks of V_{DC} in the central antenna part. For the 0/π/π/0 phasing at high P_{cen}/P_{total}, the RF image currents at the septum are in-phase and lead to higher V_{DC} in that location.

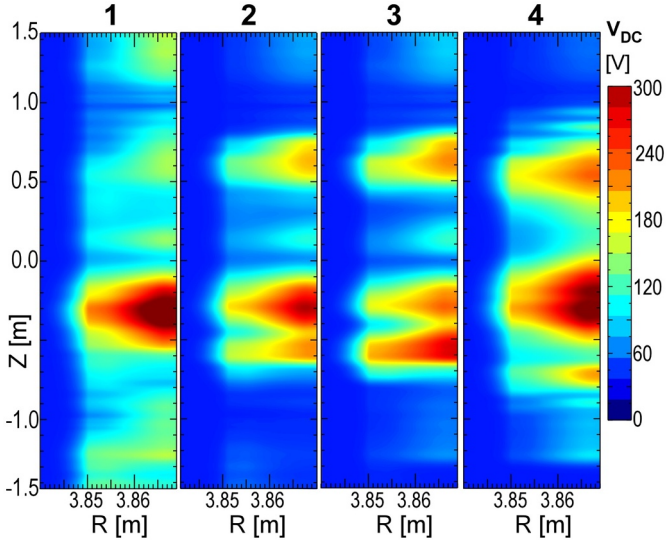

Fig. 9. Radial (R) – vertical (Z) profile of V_{DC} calculated by SSWICH-SW at the left A2 limiter for working points in 0/π/0/π ("1–3") and in 0/π/π/0 ("4") (P_{total} = 1 MW).

The SSWICH calculations for the A2 antenna were made assuming the same relative importance of the limiters and the septum acting as PFCs and the density profile in front of the septum was taken the same as in front of the limiters. However this can be different in reality due to the shorter magnetic field line connection lengths in front of the septum compared to those in front of the limiters. This can modify the effect of septum, and the experiments are needed to characterize if such modification is significant.

It should be noted that the qualitative behavior of the minima of $E_{||,RF}$ and V_{DC} is quite robust w.r.t. changes in plasma parameters. However, for accurate estimates of expected behavior of V_{DC}, precise knowledge of the density in front of PFCs is required. V_{DC} is a non-linear function of $E_{||,RF}$ and it changes behavior in the region of large radial field gradients (e.g., around R = 3.85 m in Fig. 8), defined by the density profile [74]. Estimates of V_{DC} for the A2 antenna in H-mode plasmas are in progress and will be reported in the future.

For ITER antenna, described by the 24-port TOPICA model [75] shown in Fig. 10(a), there is no PFC such as an antenna septum. Most importantly, high $E_{||,RF}$ can appear and RF sheaths can form at the antenna lateral sides, i.e., the port boundaries. We evaluate the averaged near-field $\langle E_{||,RF}\rangle$ close to the port boundaries which can be seen in Fig. 10(b), for the so-called "high-density" case at f_{ITER} = 40 MHz [76] for P_{total} = 1 MW. Both 0/π/0/π and 0/π/π/0 phasings are tested in order to minimize the RF current and the near-field at the port boundaries. The first qualitative result is that the central straps, if out-of-phase to each other, are less efficient in exciting $E_{||,RF}$ at the limiters than the central straps of the A2 antenna. This can be seen from the $\langle E_{||,RF}\rangle$ feeding diagram for 0/π/0/π for which P_{cen}/P_{total} close to 1.0 (i.e., only about 50% of maximum power is available) corresponds to the minimum of the fields. For 0/π/π/0, on the contrary, the balanced power operation (P_{cen}/P_{total} = 0.5), which is preferable as it maximizes the available power from this antenna, is favorable to reduce $\langle E_{||,RF}\rangle$ and can be recommended as a starting point for optimizing the ICRF operation in ITER with reduced impact on the SOL and PWI. Further fine-tuning will be possible once the experimental SOL profiles are available.

Concerning ICRF systems in the more distant future, several variations of concepts of the future machines like DEMO [77] currently exist; hence we limit ourselves to providing practical recommendations in the context of antenna development for a fusion reactor. The above described general guideline to reduce the impact of the ICRF power on the

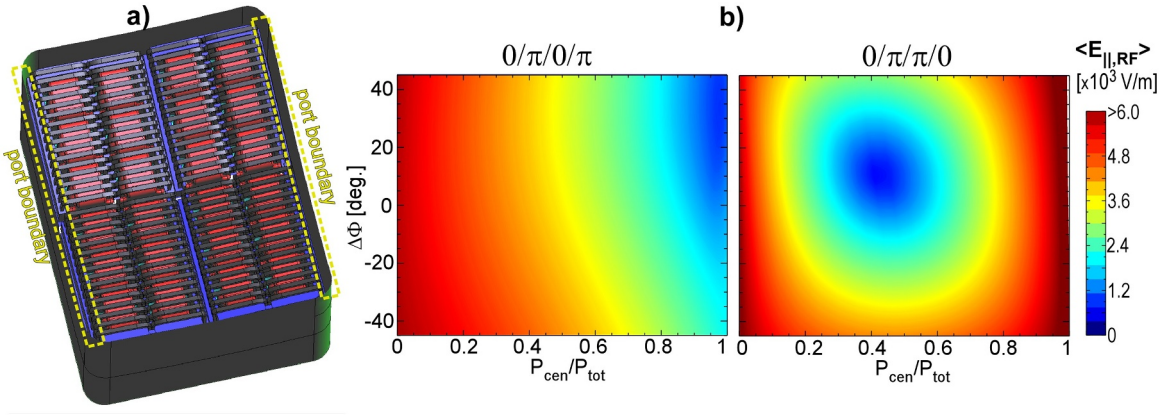

Fig. 10. (a) TOPICA model for the ITER antenna with regions close to PFCs (port boundaries) highlighted; (b) RF feeding diagrams for $E_{||,RF}$ averaged over the regions from (a) ($P_{total} = 1$ MW).

SOL and PWI can be applied both to the conventional type of antennas and the so-called travelling-wave antennas (TWAs) [78]. The conventional antenna, represented by the antennas described in this paper, use individual feeders for antenna straps, usually with minimized mutual coupling. The TWAs use fewer antenna feeders by launching a travelling wave along a structure consisting of a large number of radiating straps with increased and optimized mutual coupling.

However, for the guideline which minimizes the RF near-field in the vicinity of the PFCs to be applied, the PFC surfaces have to be well defined. In general, other antenna components (than PFCs) are not free of RF sheaths and also induce V_{DC} in a complex 3D geometry. In order for these contributions not to play an important role, these components should be: (a) retracted in the limiter shadow of the surfaces first facing the SOL plasma ("first limiting surfaces"), to assure that the plasma density is sufficiently low in the radial layer where induced V_{DC} is present; (b) the retraction should be sufficiently deep to assure a fast radial decay of V_{DC} in the shadow of the first limiting surfaces. In AUG, Alcator C-Mod and JET-ILW, the main antenna components are retracted radially in the shadow of the antenna limiters (or septum) by several centimeters. In these cases, the experimental results and the calculations indicate that the antenna limiters, and not the radially retracted structures, are the most important surfaces for the RF sheath effects. However for the future machines, it is crucial to further develop and benchmark the SOL and the RF sheath models to optimize not only the ICRF antenna, but equally important, the distribution of the PFC surfaces. The septum of the A2 antenna serves as an example of a PFC placed unfavorably for the minimization of the RF sheath effects. The design of the PFCs and their distribution requires even more attention if CD (Current Drive) phasings need to be implemented. The feeding with the CD phasings is generally not well-suited for reduction of the RF image currents, and the main guideline to reduce the currents will likely be to optimize the topology and distribution of the RF current-carrying structures including the PFCs.

4. Conclusions

Experiments in ASDEX Upgrade and Alcator C-Mod with multi-strap antennas and cancelled RF image currents at the antenna PFCs prove that mitigation, and complete elimination of the far SOL DC biasing as well as of the impurity production by ICRF sheath effects is possible, even with a high power density of up to 7 MW/m^2 and various SOL properties. The RF image cancellation technique can be aided by tailoring the 3D density distribution using local gas injection resulting in higher ICRF power capability and lower impurity source, as in ASDEX Upgrade and in JET-ILW. The density tailoring becomes more difficult if the SOL is opaque to neutrals and geometry of antenna and PFCs does not allow neutrals to distribute prior to ionization, as it is likely in the case of Alcator C-Mod. Nevertheless calculations for ITER indicate that a significant increase of the density in front of antenna is possible when using the local gas injection.

The results show that ICRF heating is compatible with a high-Z reactor wall. To build an antenna for a fusion reactor, either of the conventional type or based on the travelling-wave antenna principle, both the RF field distribution and the topology of PFCs have to be optimized. The general guideline of minimization of RF parallel electric field near PFCs including the wave fields can be used. This guideline originates from the recent experimental and theoretical studies. Considering the limited effect of wave propagation on the near-field patterns, calculations with simplified descriptions of waves are often applicable for design optimization. The assessment of the existing JET A2 antenna using the near-field and RF sheath calculations demonstrates that the placement of antenna PFCs such as septum can be unfavorable for the minimization of RF sheaths. Therefore the PFCs and their distribution have to be incorporated with antenna design at an early stage. It has been shown that in ITER, the ICRF antennas can be operated in a mode with reduced PWI, corresponding to the cancellation of the RF image currents at the antenna port boundaries, without major drawbacks on power capabilities.

Acknowledgments

This work has been carried out within the framework of the EUROfusion Consortium and has received funding from the Euratom Research and Training Programme 2014–2018 under grant agreement No. 633053. The views and opinions expressed herein do not necessarily reflect those of the European Commission. The work is supported by US DoE, Office of Science, Office of Fusion Energy Sciences, User Facility Alcator C-Mod under DE-FC02-99ER54512 and DE-SC 0010720, and under DOE Contract No. DE-AC05-00OR22725 with UT-Battelle, LLC.

References

[1] P. Jacquet, et al., "Heat loads on JET plasma facing components from ICRF and LH wave absorption in the SOL", Nucl. Fusion 51 (2011) 103018.
[2] Y. Corre, et al., "Characterization of heat flux generated by ICRH heating with cantilevered bars and a slotted box Faraday screen", Nucl. Fusion 52 (2012) 103010.
[3] S. Wukitch, et al., "RF plasma edge interactions and their impact on ICRF antenna performance in Alcator C-Mod", J. Nucl. Mater. 363–365 (2007) 491–497.
[4] S. Wukitch, et al., "Characterization and performance of a field aligned ion cyclotron range of frequency antenna in Alcator C-Mod", Phys. Plasmas 20 (2013) 056117.
[5] V. Bobkov, et al., "Assessment of compatibility of ICRF antenna operation with full W wall in ASDEX Upgrade", Nucl. Fusion 50 (2010) 035004https://iopscience.iop.org/journal/0029-5515.
[6] V. Bobkov, et al., "Making ICRF power compatible with a high-Z wall in ASDEX Upgrade", Plasma Phys. Control Fusion 59 (2017) 014022.

[7] V. Bobkov, et al., "ICRF specific plasma wall interactions in JET with the ITER-like wall", J. Nucl. Mater. 438 (2013) S160–S165.
[8] Ph. Jacquet, et al., "Ion cyclotron resonance frequency heating in JET during initial operations with the ITER-like wall", Phys. Plasmas 21 (2014) 061510.
[9] L. Colas, et al., "Self consistent radio-frequency wave propagation and peripheral direct current plasma biasing: Simplified three dimensional non-linear treatment in the "wide sheath" asymptotic regime", Phys. Plasmas 19 (2012) 092505.
[10] D. Van Eester, K. Crombé, "A crude model to study radio frequency induced density modification close to launchers", Phys. Plasmas 22 (2015) 122505.
[11] A. Lieberman, A.J. Lichtenberg, "Principles of Plasma Discharges and Materials Processing", Wiley, New York, 1994.
[12] J.-M. Noterdaeme, et al., "The ASDEX upgrade ICRH antenna", Fusion Eng. Des. 24 (1-2) (1994) 65–74.
[13] R. Ochoukov, et al., "ICRF-enhanced plasma potentials in the SOL of Alcator C-Mod", Plasma Phys. Control Fusion 56 (2014) 015004.
[14] H. Faugel, et al., "An overview of the in-vessel ICRF-diagnostics in the ASDEX Upgrade tokamak", Proceedings of the 30th Symposium on Fusion Technology, GiardiniNaxos, Italy, 2018.
[15] R. Ochoukov, "ICRF wave field measurements in the presence of scrape off layer turbulence on the ASDEX Upgrade tokamak", Rev. Sci. Instrum. 87 (2016) 11D301.
[16] J.P. Sheehan, et al., "A comparison of emissive probe techniques for electric potential measurements in a complex plasma", Phys. Plasmas 18 (2011) 073501.
[17] M. Kubic, et al., "Measurement of sheath potential in RF-biased flux tubes using a retarding field analyzer in Tore Supra tokamak", J. Nucl. Mater. 438 (2013) S509–S512.
[18] L. Colas, "2-dimensional mapping of ICRF-induced scrape-off layer modifications with a retarding field analyser on ASDEX-Upgrade", AIP Conf. Proc. 1580 (2014) 259.
[19] W. Zhang, et al., "Modelling of the ICRF induced $E \times B$ convection in the scrape-off-layer of ASDEX Upgrade", Plasma Phys. Control Fusion 58 (2016) 095005.
[20] I. Cziegler, et al., "Ion-cyclotron range of frequencies in the scrape-off-layer: fine structure radial electric fields", Plasma Phys. Control Fusion 54 (2012) 105019.
[21] R. Hong, et al., "Characterization of SOL plasma flows andpotentials in ICRF-heated plasmas in Alcator C-Mod", Plasma Phys. Control Fusion 59 (2017) 105008.
[22] C.C. Klepper, et al., "Dynamic Stark spectroscopic measurements of microwave electric fields inside the plasma near a high-power antenna", Phys Rev. Lett. 110 (2013) 215005.
[23] A. Kostic, et al., "Development of a spectroscopic diagnostic tool for electric field measurements in IShTAR (Ion cyclotron Sheath Test ARrangement)", Rev. Sci. Instrum. 89 (2018) 10D115.
[24] V. Lancellotti, et al., "TOPICA: an accurate and efficient numerical tool for analysis and design of ICRF antennas", Nucl. Fusion 46 (2006) S476–S499 https://iopscience.iop.org/journal/0029-5515.
[25] J. Jacquot, et al., "Full wave propagation modelling in view to integrated ICRH wave coupling/RF sheaths modelling", AIP Conf. Proc. 1689 (2015) 050008.
[26] V. Bobkov, et al., "Characterization of 3-strap antennas in ASDEX Upgrade", Proceeding of the EPJ Web of Conferences, 157 2017, p. 03005.
[27] A. Křivská, et al., "Electromagnetic simulations of JET ICRF ITER-like antenna with TOPICA and SSWICH asymptotic codes", Proceeding of the EPJ Web of Conferences, 157 2017, p. 03026.
[28] A. Křivská et al., "RF sheath modeling of experimentally observed plasma surface interactions with the JET ITER-Like antenna", submitted to Nuclear Materials and Energy.
[29] M.L. Garrett, S.J. Wukitch, "Mitigation of radio frequency sheaths through magnetic field-aligned ICRF antenna design", Fus. Eng. Des. 87 (2012) 1570–1575.
[30] T.G. Jenkins, D.N. Smithe, "High-performance finite-difference time-domain simulations of C-Mod and ITER RF antennas", AIP Conf. Proc. 1689 (2015) 030003.
[31] J. Jacquot, et al., "Radio-frequency sheaths physics: Experimental characterization on Tore Supra and related self-consistent modeling", Phys. Plasmas 21 (2014) 061509.
[32] L. Lu, et al., "Modelling of radio frequency sheath and fast wave coupling on the realistic ion cyclotron resonant antenna surroundings and the outer wall", Plasma Phys. Control Fusion 60 (2018) 035003.
[33] DA D'Ippolito, et al., "Modeling far-field radio-frequency sheaths in Alcator C-Mod", Plasma Phys. Control Fusion 55 (2013) 085001.
[34] R. Otin, et al., "ICRH antenna modelling with the open-source finite element tool ERMES", Proceedings of the 30th Symposium on Fusion Technology, GiardiniNaxos, Italy, 2018.
[35] S. Shiraiwa, et al., "HIS-TORIC: extending core ICRF wave simulationto include realistic SOL plasmas", Nucl. Fusion 57 (2017) 086048.
[36] S.I. Krasheninnikov, et al., "On scrape off layer plasma transport", Phys. Lett. A 283 (2001) 368–370.
[37] P. Manz, et al., "Origin and turbulence spreading of plasma blobs", Phys. Plasmas 22 (2015) 022308.
[38] C. Lau, et al., "Effects of ICRF power on SOL density profiles and LH coupling during simultaneous LH and ICRF operation on Alcator C-Mod", Plasma Phys. Control Fusion 55 (2013) 095003.
[39] V. Bobkov, et al., "ICRF operation with improved antennas in ASDEX Upgrade with W wall", Nucl. Fusion 53 (2013) 09301802004.
[40] D. Aquiam, et al., "Implementation of the new multichannel X-mode edge density profile reflectometer for the ICRF antenna on ASDEX Upgrade", Rev. Sci. Instrum. 87 (2016) 11E722.
[41] W. Zhang, et al., "Radio frequency heating induced edge plasma convection: self-consistent simulations and experiments on ASDEX Upgrade", Nucl. Fusion 57 (2017) 116048.
[42] L. Colas, et al., "Localized Scrape-Off Layer density modifications by Ion Cyclotron near fields in JET and ASDEX-Upgrade L-mode plasmas", J. Nucl. Mater. 463 (2015) 735–738.
[43] L. Colas, et al., "2D mappings of ICRF-induced SOL density modifications on JET", Proceedings of the 45th EPS Conference on Plasma Physics, Prague Czech Republic, 2018 *O4.101* http://ocs.ciemat.es/EPS2018PAP/pdf/O4.101.pdf.
[44] Y. Feng, et al., "3D edge modeling and island divertor physics", Contrib. Plasma Phys. 44 (2004) 57–69.
[45] D.A. D'Ippolito, et al., "Integrated codes for ICRF-Edge plasma interactions", AIP Conf. Proc. 787 (2005) 222.
[46] D.A. Russell, D.A. D'Ippolito, J.R. Myra, "Reduced-model simulations of turbulence and rf-driven convection in the edge and scrape-off layer plasma", Bull. Am. Phys. Soc. 49 (2004) 84.
[47] P. Tamain, et al., "Numerical analysis of the impact of an RF sheath on the Scrape-Off Layer in 2D and 3D turbulence simulations", Nucl. Mater. Energy 12 (2017) 1171–1177.
[48] J. Terry, et al., "ICRF-induced radial electric fields in the far scrape-off-layer of Alcator C-Mod", Proceedings of the 24th International Conference on Fusion Energy, San Diego, USA, 2012 EX/P5-39.
[49] M. Reinke, et al., "Experimental pathways to understand and avoid high-Z impurity contamination from ICRF heating in tokamaks", Proceedings of the 58th Annual Meeting of the American Physical Society Division of Plasma Physics, San Jose, USA, 2016.
[50] S. Wukitch, et al., "Towards ICRF antennas compatible with high performance plasmas: characterization and mitigation of ICRF aantenna – plasma edge-interactiomn", The 22nd Topical Conference on Radio-Frequency Power in Plasmas, Aix-en-Provence, France, 2017.
[51] V. Bobkov, et al., "Progress in reducing ICRF-specific impurity release in ASDEX upgrade and JET", Nucl. Mater. Energy 12 (2017) 1194–1198.
[52] S. Wukitch, et al., "ICRF specific impurity sources and plasma sheaths in Alcator C-Mod", J. Nucl. Mater. 390–391 (2009) 951–954.
[53] R. Behrisch, W. Eckstein, "Sputtering Yields", Springer-Verlag, 2007.
[54] A. Hakola, et al., "Plasma-wall interaction studies in the full-W ASDEX upgrade during helium plasma discharges", Nucl. Fusion 57 (2017) 066015.
[55] S. Brezinsek, et al., "Spectroscopic determination of inverse photon efficiencies of W atoms in the scrape-off layer of TEXTOR", Phys. Scr. T170 (2017) 014052.
[56] C.C. Klepper, et al., "RF Sheath-Enhanced Plasma Surface Interaction Studies using Beryllium Optical Emission Spectroscopy in JET ITER-Like Wall", Proceedings of the EPJ Web of Conferences, 157 2017, p. 03024.
[57] J.R. Myra, et al., "Three-dimensional analysis of antenna sheaths", Fusion Eng. Des. 31 (1996) 291.
[58] L. Colas, et al., "RF current distribution and topology of RF sheath potentials in front of ICRF antennae, Nucl. Fusion 45 (2005) 767.
[59] V. Bobkov, et al., "First results with 3-strap ICRF antennas in ASDEX Upgrade", Nucl. Fusion 56 (2016) 084001.
[60] Ph. Jacquet, et al., "ICRH physics and technology achievements in JET-ILW", Proceedings of the EPJ Web of Conferences, 157 2017, p. 02004.
[61] Ph. Jacquet, et al., "Maximization of ICRF power by SOL density tailoring with local gas injection", Nucl. Fusion 56 (2016) 046001.
[62] R. Ding, et al., "High-Z material erosion and its control in DIII-D carbon divertor", Nucl. Mater. Energy 12 (2017) 247–252.
[63] W. Zhang, et al., "3D simulations of gas puff effects on edge density and ICRF coupling in ASDEX Upgrade", Nucl. Fusion 56 (2016) 036007.
[64] W. Zhang, et al., "Effects of outer top gas injection on ICRF coupling in ASDEX Upgrade: towards modelling of ITER gas injection", Plasma Phys. Control Fusion 59 (2017) 075004.
[65] E. Lerche, et al., "Impact of localized gas injection on ICRF coupling and SOL parameters in JET-ILW H-mode plasmas", J. Nucl. Mater. 463 (2015) 634–639.
[66] V. Bobkov, et al., "Progress in controlling ICRF-edge interactions in ASDEX upgrade", AIP Conf. Proc. 1689 (2015) 030004.
[67] W. Zhang et al., "Scrape-off layer density tailoring with local gas puffing to maximize ICRF power coupling in ITER", submitted to Nuclear Materials and Energy.
[68] W. Zhang, et al., "3D simulations of gas puff effects on edge plasma and ICRF coupling in JET", Nucl. Fusion 57 (2017) 056042.
[69] V. Bobkov, et al., "Influence of gas injection location and magnetic perturbations on ICRF antenna performance in ASDEX upgrade", AIP Conf. Proc. 1580 (2014) 271.
[70] L. Colas, et al., "Spatial proximity effects on the excitation of sheath RF voltages by evanescent slow waves in the ion cyclotron range of frequencies", Plasma Phys. Control Fusion 59 (2017) 025014.
[71] F. Perkins, "Radiofrequency sheaths and impurity generation by ICRF antennas", Nucl. Fusion 29 (1989) 583.
[72] W. Tierens, et al., "Nonlinear plasma sheath potential in the ASDEX Upgrade 3-strap antenna: a parameter scan", "Nonlinear plasma sheath potential in the ASDEX Upgrade 3-strap antenna: a parameter scan" 57 (2017) 116034.
[73] D. Milanesio, et al., "Analysis of the ASDEX Upgrade 3-strap antenna with TOPICA code: Curved vs. flat 3D geometry", Proceedings of the EPJ Web of Conferences, 157 2017, p. 03034.
[74] W. Tierens, Dependence of V_DC on E_||, RF, Private Communication.
[75] D. Milanesio, R. Maggiora, "ITER ICRF antenna analysis and optimization using the TOPICA code", Nucl. Fusion 50 (2010) 025007https://iopscience.iop.org/journal/0029-5515.
[76] F. Durodié, et al., "Design, performance, and grounding aspects of the International Thermonuclear Experimental Reactor ion cyclotron range of frequencies antenna", Phys. Plasmas 21 (2014) 061512.
[77] G. Federici, et al., "European DEMO design strategy and consequences for materials", Nucl. Fusion 57 (2017) 092002.
[78] R. Ragona, A. Messiaen, "Multi-section Traveling Wave Antenna for heating of large machines as DEMO", Fusion Eng. Des. 123 (2017) 232–235.